Supporting Information for "Scale dependence of earthquake rupture prestress in models with enhanced weakening: implications for event statistics and inferences of fault stress"

Valère Lambert[1] Nadia Lapusta[1,2] Daniel Faulkner[3]

[1]Seismological Laboratory, California Institute of Technology, Pasadena, California, USA

[1,2]Department of Mechanical and Civil Engineering, California Institute of Technology, Pasadena, California, USA

[3]School of Environmental Sciences, University of Liverpool, Liverpool, UK

Contents of this file

S1. Methodology for simulations of sequences of earthquakes and aseismic slip with and without the thermal pressurization of pore fluids

In order to conduct numerical simulations of sequences of spontaneous earthquakes and aseismic slip, we utilize the spectral boundary integral method to solve the elastodynamic equations of motion with the friction boundary conditions, including the evolution of pore fluid pressure and temperature on the fault coupled with off-fault diffusion (Lapusta et al., 2000; Noda & Lapusta, 2010). Our fault models are governed by a form of the laboratory-derived Dieterich-Ruina rate-and-state friction law regularized for zero and negative slip rates, with the state evolution governed by the aging law (Rice & Ben-Zion, 1996; Noda & Lapusta, 2010). The most commonly used formulation of rate-and-state laws is the Dieterich-Ruina formulation (Dieterich, 1979; Ruina, 1983):

$$\tau = \overline{\sigma} f(V, \theta) = (\sigma - p)\left[f_* + a \ln \frac{V}{V_*} + b \ln \frac{\theta V_*}{L}\right], \tag{S1}$$

where f_* is a reference steady-state friction coefficient at reference sliding rate V_*, L is the characteristic slip distance, and a and b are the direct effect and evolution effect parameters, respectively. During steady-state sliding ($\dot{\theta} = 0$), the friction coefficient is expressed as:

$$f_{ss}(V) = f_* + (a - b) \ln \frac{V}{V_*}, \tag{S2}$$

where the combination of frictional properties $(a - b) > 0$ results in steady-state velocity-strengthening (VS) behavior, where stable slip is expected, and properties resulting in $(a - b) < 0$ lead to steady-state velocity-weakening (VW) behavior, where accelerating slip and hence stick-slip occur for sufficiently large regions.

The peak shear stress during dynamic rupture propagation can correspond to a much higher apparent friction coefficient than the reference friction coefficient f_* or the similar steady-state friction coefficient at seismic slip rates of the order of 1 m/s. Assuming that the fault has been locked interseismically with the state variable healing to a value θ_{int} and the slip rate rapidly accelerates to the peak slip rate V_{peak} upon arrival of the rupture front with negligible evolution of the state variable $\theta \approx \theta_{\text{int}}$, the peak friction can be approximately given as:

$$\begin{aligned}\tau_{\text{peak}}/(\sigma - p_{\text{int}}) &= f_* + a\ln\frac{V_{\text{peak}}}{V_*} + b\ln\frac{\theta_{\text{int}}}{\theta_{\text{ss}}(V_*)} \\ &= \frac{\tau_{\text{ss}}(V_{\text{peak}})}{(\sigma - p_{\text{int}})} + b\ln\frac{\theta_{\text{int}}}{\theta_{\text{ss}}(V_{\text{peak}})} \\ &= \frac{\tau_{\text{ss}}(V_{\text{pl}})}{(\sigma - p_{\text{int}})} + (a-b)\ln\frac{V_{\text{peak}}}{V_{\text{pl}}} + b\ln\frac{\theta_{\text{int}}}{\theta_{ss}(V_{\text{peak}})}\end{aligned} \tag{S3}$$

Note that $V_{\text{peak}} \gg V_* \gg V_{\text{pl}}$ and $\theta_{\text{int}} \gg \theta_{\text{ss}}(V_*) \gg \theta_{\text{ss}}(V_{\text{peak}})$ for typical seismic slip rates and interseismic durations of healing. The last two terms on the third line gives the difference between the local SSQS shear resistance described in the main text and the peak shear resistance, where the last term typically dominates for periods of extending healing and higher values of θ_{int}. Consequently, for a given dynamic slip rate V_{peak}, the better healed the interface with higher θ_{ini}, the higher the peak friction during dynamic rupture (Lambert & Lapusta, 2020).

The standard Dieterich-Ruina formulation (equation S1) has been empirically-determined from laboratory experiments at sliding rates between 10^{-9} m/s to around 10^{-3} m/s. Under the standard logarithmic formulation, friction becomes negative as the slip rate V approaches zero and is undefined for zero or negative slip rates (Figure S5). The standard formulation may be regularized near $V = 0$ such that the shear resistance remains positive for all positive values of V (Rice & Ben-Zion, 1996):

$$\tau(V,\theta) = a\overline{\sigma}\sinh^{-1}\left[\frac{V}{2V_*}\exp\left(\frac{f_* + b\log(\theta V_*/L)}{a}\right)\right], \tag{S4}$$

with the steady-state shear resistance given by:

$$\tau_{ss}(V) = a\overline{\sigma}\sinh^{-1}\left[\frac{V}{2V_*}\exp\left(\frac{f_* + b\log(V_*/V)}{a}\right)\right]. \tag{S5}$$

Theoretical justification for such regularization has been provided by drawing analogy between the direct velocity effect and the exponential formulation of thermally-activated creep at contact junctions, where the contact shear stress acts as a biasing factor (Rice et al., 2001). The standard logarithmic rate-dependent formulation is derived when only considering forward activated jumps, which may be dominant under significant shear stress and conditions relevant to most laboratory experiments. The regularized formulation (equation S4) arises when including the presence of backward jumps, which are equally probable as forward jumps for $\tau = 0$, as in the full thermally-activated creep theory. The logarithmic and regularized formulations are equivalent for conditions consistent with laboratory experiments, and differ only for very low slip rates (Figure S5).

Earthquakes may nucleate only if the VW region is larger than the nucleation size h^*. For 2D problems, two theoretical estimates of the nucleation size in mode III are (Rice & Ruina, 1983; Rubin & Ampuero, 2005):

$$h^*_{RR} = \frac{\pi}{4}\frac{\mu L}{(b-a)(\sigma - p)};\; h^*_{RA} = \frac{2}{\pi}\frac{\mu L b}{(b-a)^2(\sigma - p)}, \tag{S6}$$

where μ is the shear modulus. The simulated fault in our models contains a 24-km region with VW frictional properties surrounded by VS regions to create a 72-km frictional region. Outside of this frictional regions, the fault moves with a prescribed plate rate V_{pl} to provide tectonic-like loading (Figure 2A of main text).

The thermal pressurization of pore fluids is governed in our simulations by the following coupled differential equations for temperature and pore pressure evolution (Noda & Lapusta, 2010):

$$\frac{\partial T(y,z;t)}{\partial t} = \alpha_{\mathrm{th}}\frac{\partial^2 T(y,z;t)}{\partial y^2} + \frac{\tau(z;t)V(z;t)}{\rho c}\frac{\exp(-y^2/2w^2)}{\sqrt{2\pi}w}, \tag{S7}$$

$$\frac{\partial p(y,z;t)}{\partial t} = \alpha_{\mathrm{hy}}\frac{\partial^2 p(y,z;t)}{\partial y^2} + \Lambda\frac{\partial T(y,z;t)}{\partial t}, \tag{S8}$$

where T is the temperature of the pore fluid, α_{th} is the thermal diffusivity, τV is the shear heating source distributed over a Gaussian shear layer of half-width w, ρc is the specific heat, y is the distance normal to the fault plane, α_{hy} is the hydraulic diffusivity, and Λ is the coupling coefficient that gives pore pressure change per unit temperature change under undrained conditions. To approximate the effects of off-fault yielding we employ a velocity limit of $V_{\mathrm{max}} = 15$ m/s, as discussed in detail in Lambert et al. (in press). This approximation is motivated by detailed dynamic rupture simulations with off-fault yielding (Andrews, 2004), with the value of velocity limited corresponding to a representative seismogenic depth of 10 km.

Our simulations include fault models with varying levels of ambient fluid overpressure in terms of effective normal stress and as well as degrees of efficiency due to enhanced weakening due to thermal pressurization. Parameters for the simulations are given in Tables 1-3. Note that the stress changes associated with standard rate-and-state friction have a relatively mild logarithmic dependence on slip rate and are directly proportional to the effective confining stress. As such, persistently weak rate-and-state fault models with low effective normal stress and no enhanced weakening result in generally mild static stress drops (≤ 2 MPa) for typical frictional parameters measured in the laboratory (Figure 2 of main text). Thus, the inclusion of at least mild enhanced dynamic weakening is required for fault models with low effective normal stress, such as due to substantial fluid overpressurization, to produce average static stress drops between 1 - 10 MPa, as typically inferred for natural earthquakes (Figures 11 of main text and S3; Lambert et al., in press).

In order to examine the prestress at the beginning of dynamic ruptures, we define the beginning and end of dynamic rupture, as well as the ruptured area, based on a slip velocity threshold ($V_{\mathrm{thresh}} = 1$ cm/s) for seismic slip. We have found in previous studies that varying V_{thresh} between by 10^{-3} to 10^{-1} m/s results in minor variations of the determined rupture timing and area, within 1% (Perry et al., 2020; Lambert et al., in press).

Our fault models with more efficient enhanced dynamic weakening produce fewer smaller events than those with mild to moderate enhanced weakening, as can be observed in the frequency-magnitude statistics (Figure 10 of the main text). To create frequency-magnitude histograms we compute the seismic moment $M_0 = \mu A \overline{\delta}$ for ruptures, where μ is the shear modulus, A is the rupture area and $\overline{\delta}$ is the average slip in the rupture. As our simulations are 2-D, we compute the moment by assuming a circular rupture area $A = \pi(\lambda_{\mathrm{rupt}}/2)^2$, where λ_{rupt} is the rupture length.

S2. Single-degree-of-freedom representation of laboratory experiments

We compare the evolution of local slip rate and shear stress in our simulated dynamic ruptures with single-degree-of-freedom (SDOF) calculations motivated by high-velocity laboratory experiments that impose variable seismic slip rates to infer shear resistance evolution and often compare their findings with seismological observations (Sone & Shimamoto, 2009; Fukuyama & Mizoguchi, 2010). The SDOF calculations are governed by the same rate-and-state friction with enhanced dynamic weakening due to thermal pressurization as in our fault model TP4. Our SDOF calculations impose a slip-rate history, as typically done in laboratory experiments, and solve for the evolution of shear stress, state variable, temperature and pore pressure using equation 3 of the main text and equations S4 and S7-8 given the initial state. We assume initial conditions where sliding has been maintained until steady-state conditions at the slip rate of $V = 0.1$ mm/s, comparable to the initial conditions of Fukuyama and Mizoguchi (2010). We then impose two different slip rate functions characterized by regularized Yoffe functions (Tinti et al., 2005), with total slip of 1.95 m (comparable to our simulated slip) and maximum slip rate of 2 m/s. Tinti et al. (2005) regularized the stress singularity in the analytical Yoffe function by convolving it with a triangular function of half-width t_s. The regularized Yoffe functions are characterized by two time-scales, the half-width t_s and the rise time t_r. For the two examples shown in Figure 9 of the main text, we choose values of $t_r = 3$s with $t_s = 0.1t_r$ for RYF1 and $t_r = 1.4$s with $t_s = 0.4t_r$ for RYF2, in order to compare pulses with more pronounced and gradual accelerations that produce the same slip and peak slip rate.

References

Andrews, D. J. (2004, 06). Rupture Models with Dynamically Determined Breakdown Displacement. *Bulletin of the Seismological Society of America*, *94*(3), 769-775. doi: 10.1785/0120030142

Dieterich, J. H. (1979). Modeling of rock friction 1. experimental results and constitutive equations. *Journal of Geophysical Research*, *84*(B5), 2161-2168.

Fukuyama, E., & Mizoguchi, K. (2010). Constitutive parameters for earthquake rupture dynamics based on high-velocity friction tests with variable sliprate. *International Journal of Fracture*, *163*(1), 15–26. doi: 10.1007/s10704-009-9417-5

Lambert, V., & Lapusta, N. (2020). Rupture-dependent breakdown energy in fault models with thermo-hydro-mechanical processes. *Solid Earth*, *11*(6), 2283–2302. doi: 10.5194/se-11-2283-2020

Lambert, V., Lapusta, N., & Perry, S. (in press). Propagation of large earthquakes as self-healing pulses and mild cracks. *Nature*.

Lapusta, N., Rice, J. R., Ben-Zion, Y., & Zheng, G. (2000). Elastodynamic analysis for slow tectonic loading with spontaneous rupture episodes on faults with rate- and state- dependent friction. *Journal of Geophysical Research*, *105*, 765-789. doi: 10.1029/2000JB900250

Noda, H., & Lapusta, N. (2010). Three-dimensional earthquake sequence simulations with evolving temperature and pore pressure due to shear heating: Effect of heterogeneous hydraulic diffusivity. *Journal of Geophysical Research*, *115*, B123414. doi: 10.1029/2010JB007780

Perry, S. M., Lambert, V., & Lapusta, N. (2020). Nearly magnitude-invariant stress drops in simulated crack-like earthquake sequences on rate-and-state faults with thermal pressurization of pore fluids. *Journal of Geophysical Research: Solid Earth*, e2019JB018597. doi: 10.1029/2019JB018597

Rice, J. R., & Ben-Zion, Y. (1996, 04). Slip complexity in earthquake fault models. *Proceedings of the National Academy of Sciences of the United States of America*, *93*(9), 3811–3818. doi: 10.1073/pnas.93.9.3811

Rice, J. R., Lapusta, N., & Ranjith, K. (2001). Rate and state dependent friction and the stability of sliding between elastically deformable solids. *Journal of the Mechanics and Physics of Solids*, *49*(9), 1865-1898.

Rice, J. R., & Ruina, A. L. (1983). Stability of steady frictional slipping. *Journal of Applied Mechanics*, *50*(2), 343-349.

Rubin, A., & Ampuero, J.-P. (2005). Earthquake nucleation on (aging) rate and state faults. *Journal of Geophysical Research: Solid Earth*, *110*(B11).

Ruina, A. (1983). Slip instability and state variable friction laws. *Journal of Geophysical Research*, *88*(B12), 10359-10370.

Sone, H., & Shimamoto, T. (2009). Frictional resistance of faults during accelerating and decelerating earthquake slip. *Nature Geoscience*, *2*(10), 705–708. doi: 10.1038/ngeo637

Tinti, E., Fukuyama, E., Piatanesi, A., & Cocco, M. (2005). A Kinematic Source-Time Function Compatible with Earthquake Dynamics. *Bulletin of the Seismological Society of America*, *95*(4), 1211-1223. doi: 10.1785/0120040177

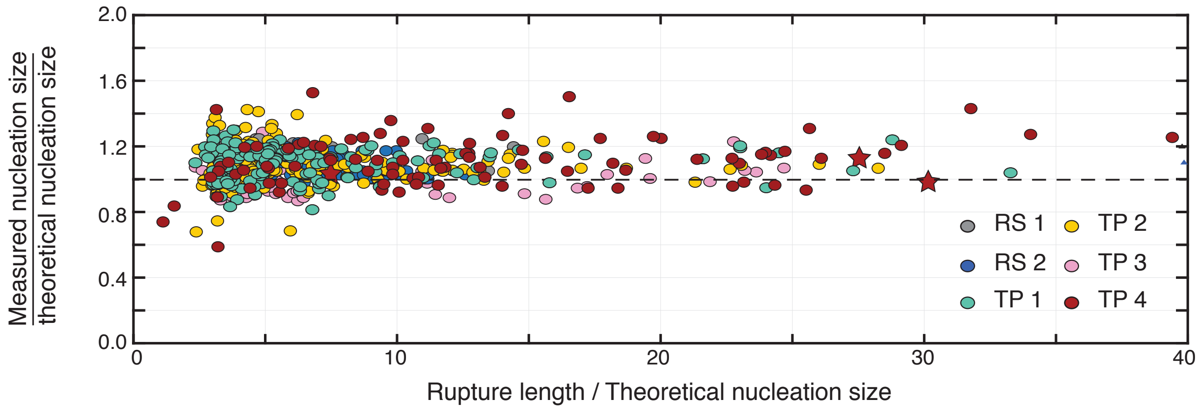

Figure S1. The measured nucleation sizes of the simulated ruptures are comparable to the theoretical estimate h^*_{RA}, within a factor of 2.

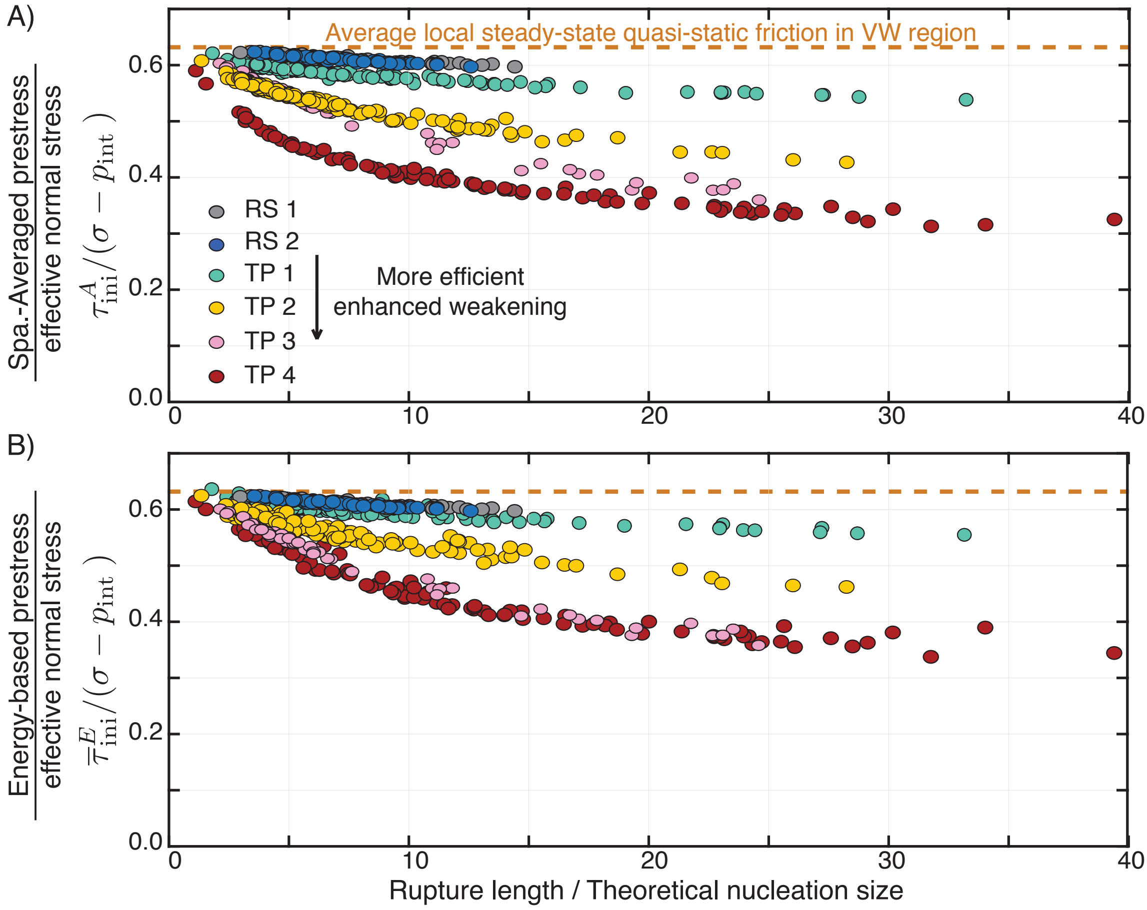

Figure S2. The spatially-averaged prestress $\tau^A_{\rm ini}$ and energy-averaged prestress $\overline{\tau}^E_{\rm ini}$ are generally comparable and decrease with increasing rupture size and efficiency of weakening.

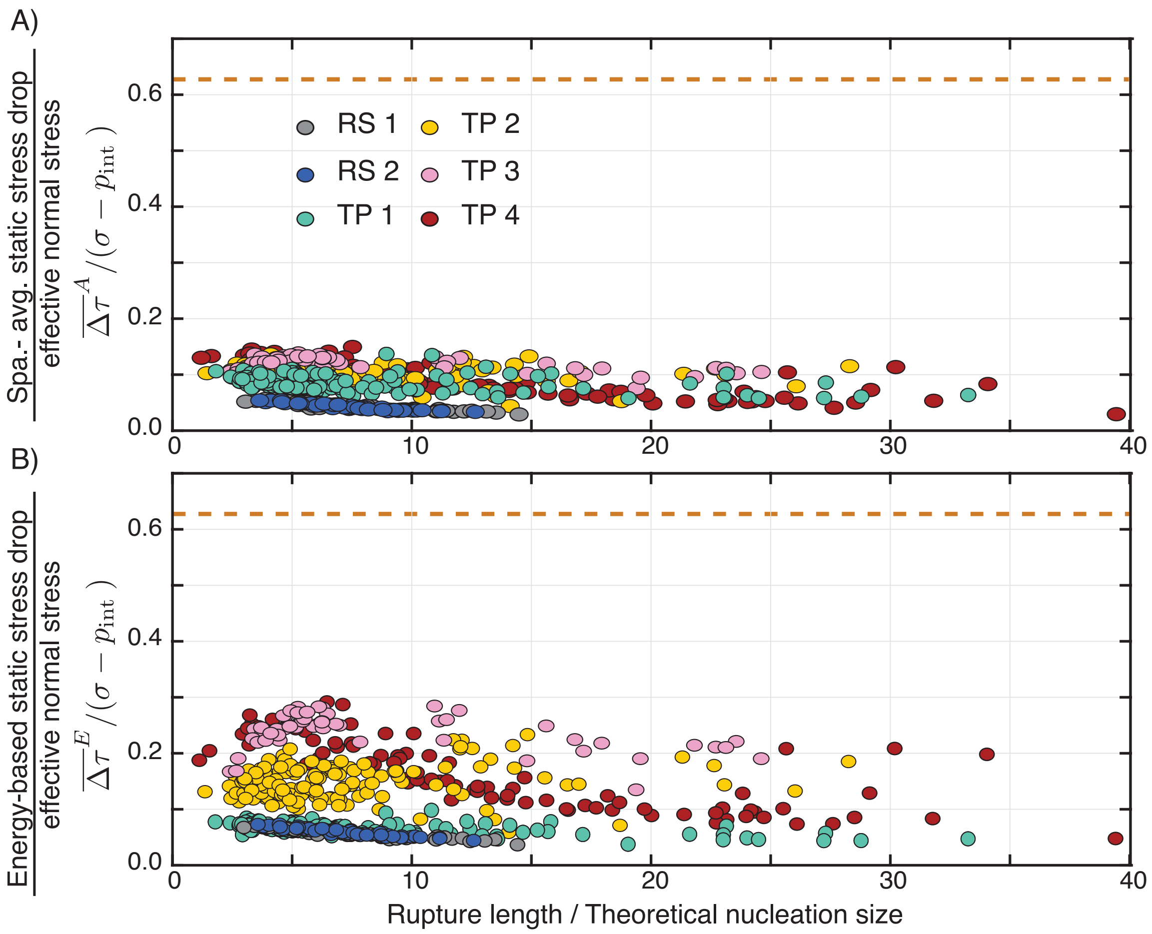

Figure S3. The (A) spatially-averaged and (B) energy-based average static stress drops for ruptures represent relatively mild decreases in average shear stress with respect to the effective normal stress. Persistently weak fault models with low effective normal stress $\leq$ 20 MPa and relatively mild weakening, such as from standard rate-and-state friction (RS1 and RS2) produce potentially too small average static stress drops $\leq$ 2 MPa, whereas models with mild to moderate enhanced weakening (TP1-4) produce realistic average static stress drops of 1 - 10 MPa.

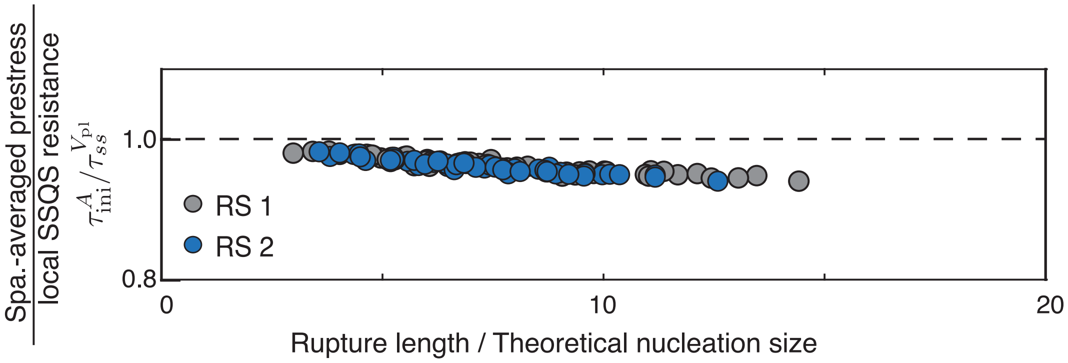

Figure S4. Ruptures on fault models with relatively mild weakening due to standard rate-and-state friction also exhibit a mild decrease in the spatially-averaged prestress $\tau_{\rm ini}^{A}$ with increasing rupture size.

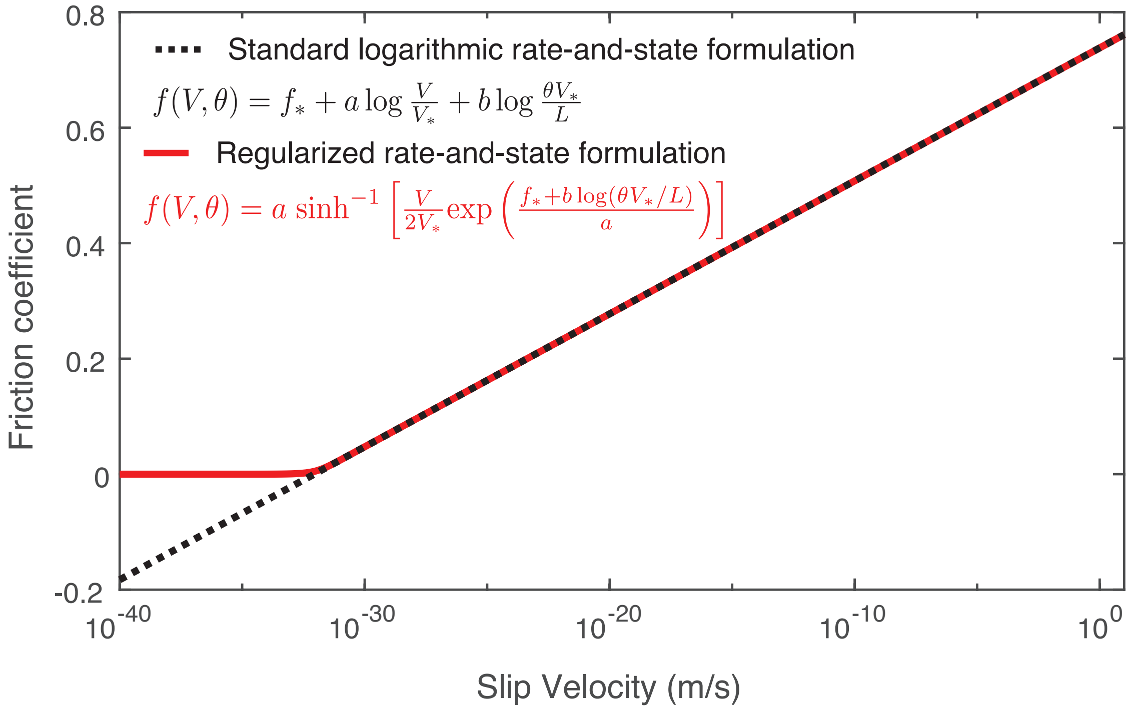

Figure S5. Comparison of the standard logarithmic (black) and regularized (red) formulations for rate-and-state friction given fixed $\theta = L/V_*$ with $V_* = 1$ μm/s, $f_* = 0.6$, and $(a - b) = 0.004$. The two formulations are equivalent for slip rates relevant to most laboratory experiments but differ as V approaches 0 m/s.